BILINGUAL PUBLISHING GROUP

Non-Metallic Material Science

https://journals.bilpubgroup.com/index.php/nmms

ARTICLE

Investigation of Dielectric Properties of Quaternary Ceramic 0.47BNT-0.04BT-0.37PMN-0.18PT

Aparna Saxena[1], Abhilash J. Joseph[2], Raghvendra Sahai Saxena[3*]

[1] *Hindu College, University of Delhi, Delhi 110007, India*

[2] *University of Delhi, Delhi 110007, India*

[3] *Solid State Physics Laboratory, Lucknow Road, Timarpur, Delhi-110054, India*

ABSTRACT

Dielectric dispersion analysis has been carried out for the first time on a new quaternary ceramic [0.47($Bi_{0.5}Na_{0.5}$)TiO_3-0.04$BaTiO_3$-0.31$Pb(Mg_{1/3}Nb_{2/3})O_3$-0.18$PbTiO_3$] having a morphotropic phase boundary composition. The measurement of the dielectric parameters has been carried out in the frequency range of 200 Hz to 2 MHz and temperature range from 30 °C to 300 °C. The material showed high dielectric constant, low dielectric loss, negligible DC conductivity and high ferroelectric to paraelectric transition temperature. A clear Debye type relaxation was observed in the dielectric constant and dielectric loss data. An interesting feature of two Debye peaks has been noticed in dielectric loss versus frequency curves in the temperature range 125 °C to 175 °C. These peaks shift towards higher frequencies when temperature is increased. The extracted relaxation times of the two peaks are three orders of magnitude different and have been found to follow the Arrhenius law with significantly different activation energies.

Keywords: BNT-BT, Debye dispersion, PMN-PT, Quaternary ceramic

1. Introduction

The relaxor type ferroelctric PMN-PT (lead magnesium niobate - lead titanate) is one of the most studied binary system, which is recognized for excellent dielectric, piezoelectric, pyroelectric and ferroelectric properties [1–13]. High dielectric constant in these materials provides advantage in many device applications including multilayer capacitors, actuators, sensors and transducers etc.. These

*CORRESPONDING AUTHOR:

Raghvendra Sahai Saxena, Solid State Physics Laboratory, Lucknow Road, Timarpur, Delhi-110054, India; Email: rs_saxena@yahoo.com

ARTICLE INFO

Received: 24 February 2024 | Revised : 26 March 2024 | Accepted: 27 March 2024 | Published Online: 17 April 2024

DOI: https://doi.org/10.30564/nmms.v5i2.6271

CITATION

O, 2024. Investigation of Dielectric Properties of Quaternary Ceramic 0.47BNT-0.04BT-0.37PMN-0.18PT. Non-Metallic Material Science. 5(2): 26–36. DOI: https://doi.org/10.30564/nmms.v5i2.6271

binary solid solutions exhibit excellent ferroelectric properties near morphotropic phase boundary (MPB). Another important ferroelectric material that is gaining interest in research and in various applications is BNT-BT (bismuth sodium titanate – barium titanate) due to its less toxicity, high Curie temperature, excellent ferroelectric, piezoelectric and ferroelectric properties along with the absence of undesired pyroclore phase [14–20].

To explore the combined advantages of both PMN-PT and BNT-BT, a quaternary solid state solution with MPB composition, [0.47($Bi_{0.5}Na_{0.5}$)TiO_3-0.04$BaTiO_3$-0.31$Pb(Mg_{1/3}Nb_{2/3})O_3$-0.18$PbTiO_3$], denoted hereafter as 0.47BNT-0.04BT-0.31PMN-0.18PT, has been synthesized in-house for the first time using solid state reaction method as explained earlier [21]. In our earlier work, we performed detailed micro-structural, ferroelectric, piezoelectric and dielectric characterization of the material and found absence of resistive leakage in this material, high transition temperature of 190 ^oC and high coercive field of 16.56 $kVcm^{-1}$ [21]. These properties were found to be significantly better than those of the pure PMN–PT ceramic reported earlier [6, 22]. This material, in addition to providing enhanced material properties, leads to the elimination of pyrochlore phase. It also reduces lead content and toxicity that is important in consumer electronics applications.

The excellent properties of 0.47BNT-0.04BT-0.31PMN-0.18PT make this material suitable for usage in high temperature and high field applications. This can be used as a high K (high dielectric permittivity) dielectric material in many applications. Therefore, the exploration of its dielectric behaviour with varying frequency and temperature is important. Furthermore, since in most of the applications these materials undergo repeated switching in the applied electric field and may face degradation in their properties, the variations in dielectric properties with target operating conditions need to be understood very well before using them in specific applications. Dielectric permittivity gets affected by the polarizations due to electronic, ionic, dipolar and space charge mechanisms in the material. These polarization contributions relax in different frequency regions and provide information about the interactions present among various species [23]. Dielectric dispersion is a strong tool to observe these relaxations. Thus, study of dielectric dispersion of a material is very important from the device application point of view. It is also interesting to identify whether the Debye type relaxations continues to exist in higher range of temperatures or it is due to the ferroelectric to paraelectric phase transition.

In this paper, we present a detailed analysis of the dielectric properties of 0.47BNT-0.04BT-0.31PMN–0.18PT quaternary material system that shows many Debye type relaxations in ferroelectric as well as in paraelectric phase. The investigation of dielectric dispersion was carried out in the light of Debye model with a distribution of relaxation time.

2. Experimental Details

A quaternary ceramic material 0.47BNT–0.04BT–0.31PMN–0.18PT with MPB composition has been synthesized using solid state reaction method. A detailed characterization of the material has been performed, such as microstructural analysis using scanning electron microscopy (Model EVO 50, Zeiss) followed by X-ray diffraction performed on the sintered pellets of the material on RIGAKU ULTIMA-IV X-ray difractometer with Cu Kα radiation (λ=1.5405Å) for structural analysis. The bulk density was measured using Archimedes principle with distilled water. The ferroelectric hysteresis analysis using RADIANT PRECISION LCII ferroelectric tester (Model No. P-HVi210KSC), displacement versus voltage curve plots using fiber optic displacement sensor (photonic sensor) by MTI Instruments Inc. have also been performed. All the characterization results and analysis are reported in our earlier work [21].

For dielectric properties, reported in this paper, the sample of this material has been mounted in Agilent's 16048A sample holder and dielectric parameters were measured as function of frequency

and temperature using Agilent's LCR meter, E4890A. These measurements were performed in the frequency range 200 Hz – 2 MHz with the temperature sweep in the range 30°C – 300°C.

3. Results and Discussion

The material shows a high dielectric constant, low dielectric loss and very low DC conductivity, making it attractive in many applications. However, these parameters show variations with respect to frequency and temperature that need to be investigated for efficient device design. The frequency dependence of dielectric permittivity is governed by various polarization mechanisms as depicted in **Figure 1** [24]. This frequency dependence changes with the temperature in most of the ceramic materials. As the temperature increases, the oxygen vacancies in the material increase resulting in creation of more dipoles. Also, the relaxation time decreases with increasing temperature because relaxation time of dipole polarization is much lower than that of the ionic and space charge polarization.

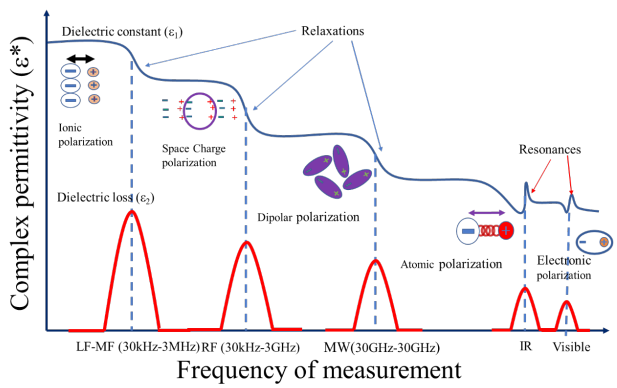

Fig. 1: Frequency dependence of dielectric permittivity and associated mechanisms.

Source: Volkov, A. A., Prokhorov, A. S.[24].

3.1. Temperature and Frequency Dependence of Dielectric Permittivity in BNT-BT PMN-PT Material

The real and imaginary parts of the measured dielectric permittivity (also known as dielectric constant and dielectric loss, respectively) are shown as surface plots in **Figure 2(a)** and **(b)**, respectively with respect to frequency and temperature. The anomalies in frequency dependence of dielectric parameters are associated with dynamics of polarized species, while the anomalies in temperature dependence is associated with formation of polar regions in relaxor ferroelectric. As evident from the surface plots, the dielectric constant in this material reduces when the frequency of measurement is increased, while with respect to temperature, it shows a peak. The dielectric loss has a different trend as compared to the dielectric constant. It shows peaks with respect to both the frequency and the temperature.

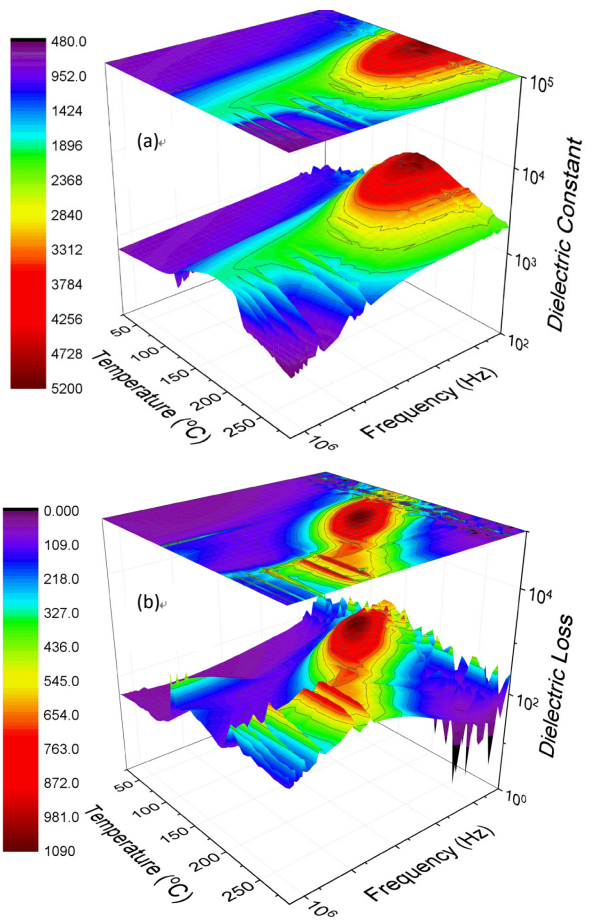

Fig. 2: Surface plot of dielectric measurement data as function of frequency and temperature, (a) Dielectric constant, (b) Dielectric loss.

The material shows high dielectric constant and also shows low dielectric loss at room temperature compared to conventional material systems, making

it a very attractive dielectric material. In most of the applications, high dielectric constant and low dielectric loss in the entire range of operating conditions are desirable characteristics. Therefore, using the plots shown in **Fig. 2(a)** and **(b)**, we examined the material its best operating conditions and investigated how the performance deviates when operating frequency and temperature are varied. We notice that the low frequency dielectric constant increases with increasing temperature till it attains its maximum value of 4140 at about 175 °C temperature. A further increase in temperature results in the reduction in its value although it remains sufficiently high even up to about 200 °C temperature.

For further investigation, the dielectric constant for some selected frequencies has been plotted as function of temperature, which is shown in **Fig. 3(a)**. The dielectric constant versus temperature curves show a peak whose value reduces with increasing frequency. The location of this peak also shifts with respect to temperature but it remains between 170 °C and 200 °C and does not show any clear direction of shift. The dielectric dispersion starts becoming significant at about 125 °C temperature as evident from the **Fig. 3(b)**, which displays dielectric constant versus frequency curves for selected temperatures of measurement. Two distinct negative slope regions separated by a kind of plateau are visible in dielectric constant versus frequency curves. This indicates that there are two frequency regions showing change in dielectric permittivity. This behaviour of dielectric dispersion found in the low frequency range of 200 Hz – 55 kHz is due to the space charge contribution and is similar to the dispersion found at high frequency, i.e., >1 MHz which is due to dipole polarization. When the temperature is increased, the thermal energy is acquired by the polarized species and results in their increased motion. This results in the reduction in the relaxation time and in the shifting of dispersion characteristics towards the relatively higher frequencies.

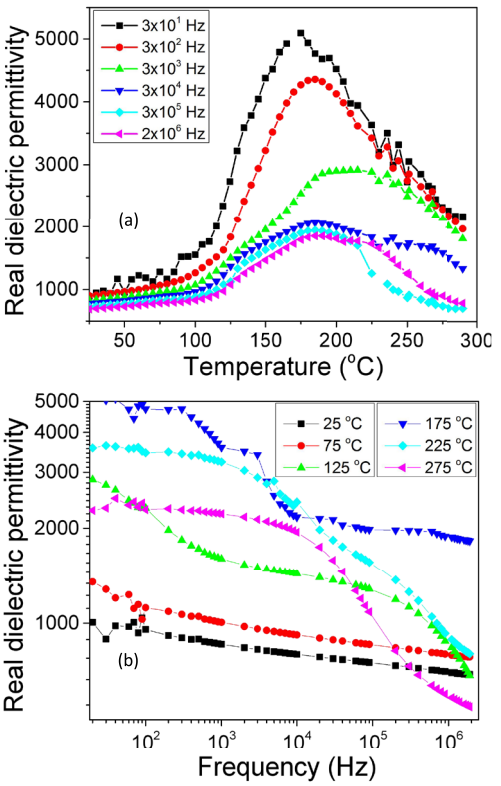

Fig. 3: (a) Dielectric constant versus temperature curves for different frequencies, **(b)** Dielectric versus frequency curves measured at different temperatures.

3.2. Fitting with Debye Model and Extraction of Parameters

The measured dielectric loss data has been found to have peaks as function of frequency associated with the steep negative slope region of the dielectric constant. This is a clear indication of the Debye type behaviour [25–27]. Therefore, the dielectric response has been analyzed based on the Debye relaxation model equations, equation (1) – (4) [22, 27].

$$\varepsilon^{*} = \varepsilon' - \varepsilon'' \tag{1}$$

$$\varepsilon' = \varepsilon_{\infty} + \Delta\varepsilon \frac{1+(\omega\tau)^{1-\alpha}\sin(\alpha\pi/2)}{1+2(\omega\tau)^{1-\alpha}\sin(\alpha\pi/2)+(\omega\tau)^{2(1-\alpha)}} \tag{2}$$

$$\varepsilon'' = \frac{\sigma_{dc}}{\varepsilon_0\omega} + \Delta\varepsilon \frac{1+(\omega\tau)^{1-\alpha}\cos(\alpha\pi/2)}{1+2(\omega\tau)^{1-\alpha}\sin(\alpha\pi/2)+(\omega\tau)^{2(1-\alpha)}} \tag{3}$$

$$\sigma = \sigma_{dc} + \omega\varepsilon_0\Delta\varepsilon \frac{1+(\omega\tau)^{1-\alpha}\cos(\alpha\pi/2)}{1+2(\omega\tau)^{1-\alpha}\sin(\alpha\pi/2)+(\omega\tau)^{2(1-\alpha)}} \tag{4}$$

Here, ε^* is the complex permittivity, while ε' and ε" are the real and imaginary parts of the dielectric permittivity, respectively. ω is the angular frequency of measurement in rad/s, σ is electrical conductivity, ε_∞ is the intrinsic permittivity and ε_0 is DC permittivity. The difference between the intrinsic and the DC permittivity is dipolar relaxation strength, denoted here as Δε. τ is the relaxation time and α is the Debye distribution parameter of relaxation times. σ_{dc} is DC conductivity in the material, which appears in the dielectric loss expression. The DC conductivity causes a steep rise in the dielectric loss curve with reducing frequency in low frequency regime, which is absent in the surface plot of dielectric loss shown in **Figure 2(b)**. Therefore, we conclude that the DC conductivity is negligible in the material and we ignored it in the fitting of the dielectric loss data. The dielectric constant and dielectric loss data as function of angular frequency has been fitted with **equation (2)** and **equation (3)** for selected temperatures. We found an excellent simultaneous fitting of both the parameters with the Debye model as shown in **Figures 4(a-h)**. The dielectric loss versus frequency curves have shown different behaviour in different temperature range. No peak is observed at lower temperature, i.e., at 55 ^oC as depicted in **Figure 4(a)**. Double peaks in the temperature range 125 ^oC to 150 ^oC have been observed, and therefore, they have been fitted separately in two different bands of frequencies, as may be seen in **Figures 4(b-d)**. The values of fitting parameters and the observed relaxation time obtained directly from the peak frequency (using the relation $\omega_p.\tau=1$, where ω_p is the angular frequency associated with the peak in dielectric loss) are listed in Table 1. The extracted relaxation time is found to be in close agreement with the observed values within the acceptable experimental error. At higher temperatures, i.e., for above 200 ^oC, only single peaks have been observed as shown in **Figures 4(e-h)**.

The two peaks observed in the dielectric loss versus frequency data correspond to the two dispersions in the material, being a mix of relaxor type PMN-PT and normal ferroelectric BNT-BT. These peaks correspond to the dielectric dispersion contributed by the space charge and dipolar polarization. They move towards higher frequencies with increasing temperatures due to the higher thermal energy acquired by the polarized species at higher temperature.

The Debye distribution parameter, α has significantly higher values in 2nd peak as compared to that of the 1st peak, indicating that the high frequency peak is broader as compared to the low frequency peak.

Table 1: Fitting parameter values extracted by fitting the dielectric constant and loss data simultaneously using Debye model equations (2) and (3).

	Temp (oC)	Peak w.r.t. temp	Extracted parameters from fitting				Observed relaxation time
			α	τ (s)	Δε	ε∞	τ (s)=1/ωp
Ferroelectric Phase	125	1st peak	0.312	0.0018	1803.6	1411.7	0.0054
		2nd peak	0.488	1.2E-7	1289.2	145.0	1.22E-7
	135	1st peak	0.282	0.0013	2050.5	1498.5	0.0012
		2nd peak	0.685	7.99E-8	1048.0	644.0	9.43E-8
	150	1st peak	0.279	0.0005	2899.9	1676.9	0.0005
		2nd peak	0.670	2.3E-8	1109.0	800.0	7.12E-8
	200	1st peak	0.291	8.1E-5	2712.7	1811.6	7.8E-5
Paraelectric Phase	230	1st peak	0.422	9.2E-6	2723.8	624.6	9.1E-6
	250	1st peak	0.369	5.39E-6	2247.3	566.1	5.43E-6
	290	1st peak	0.466	3.43E-6	1698.9	374.4	3.23E-6

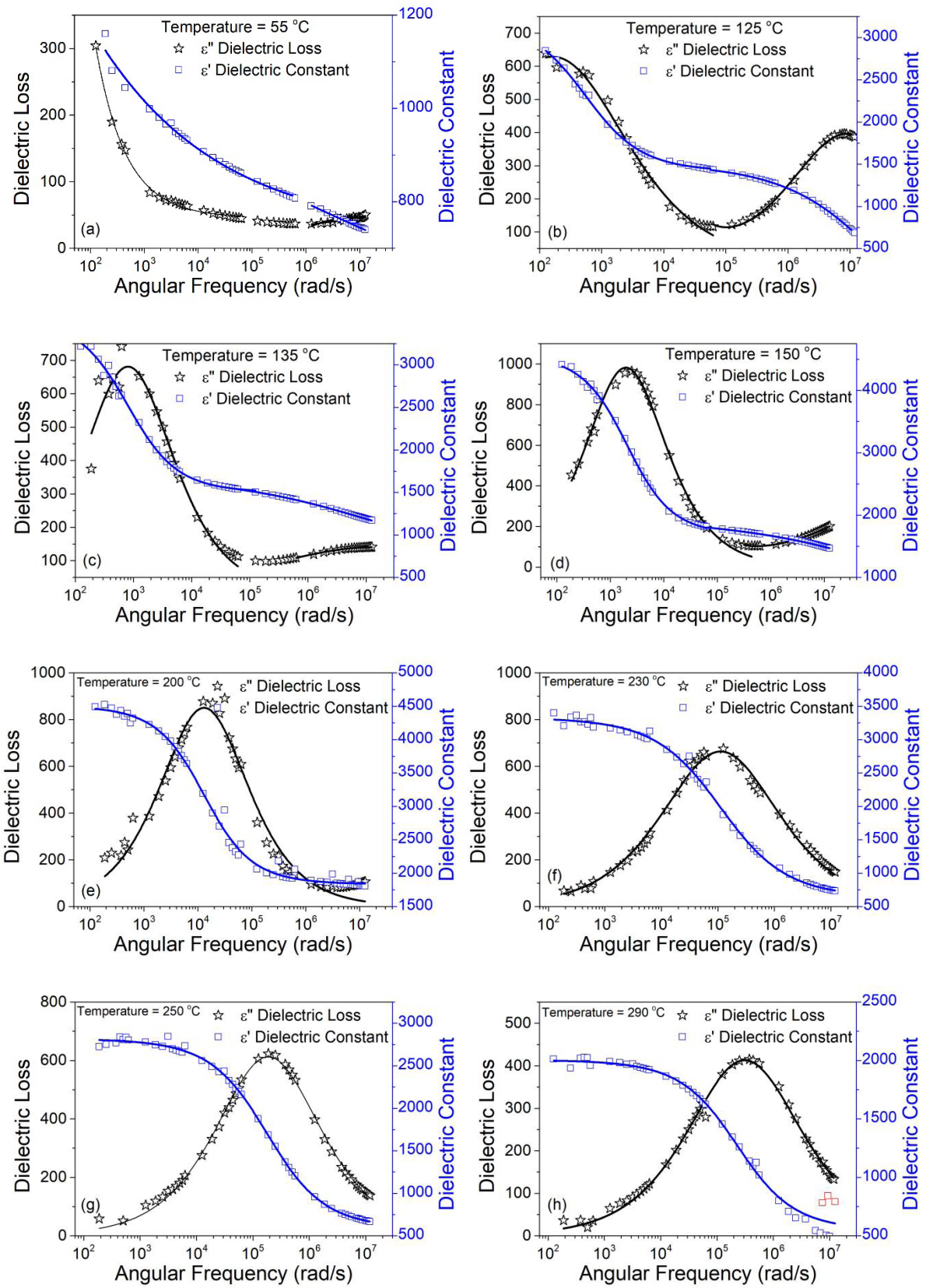

Fig. 4: Dielectric parameters as functions of frequency for different temperatures: (a) 55 °C, (b) 125 °C, (c) 135 °C, (d) 150 °C, (e) 200 °C, (f) 230 °C, (g) 250 °C, (h) 290 °C.

3.3. Relaxation Time

The relaxation times associated with these peaks also have significantly different values as displayed in Table 1. The logarithm of the relaxation time has been plotted as function of 1000/T and is found to follow the Arrhenius relation, shown in **equation (5)**.

$$\tau = \tau_0 \exp\left(\frac{\Delta E}{KT}\right) \tag{5}$$

Here ΔE is the activation energy, τ_0 is characteristics relaxation time, T is temperature and K is Boltzmann constant. The activation energy has been calculated from the slope of the Arrhenius plot, shown in **Figure 5** and the characteristic relaxation time has been calculated from its intercept with the Y-axis. The characteristic relaxation time of the low frequency peak is found to be 2.91 μs and that for the high frequency peak is 4.39 ns. For the first peak, the activation energy of relaxation time is found to be 0.344 eV, whereas for second peak it is 0.424 eV.

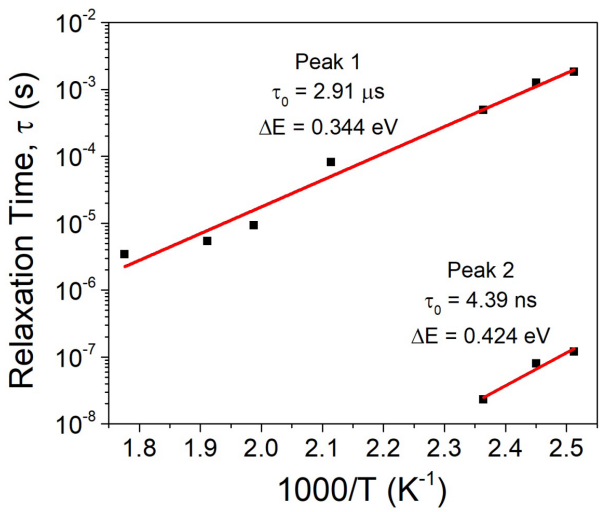

Fig. 5: The relaxation time as function of 1000/T corresponding to the two peaks observed in dielectric loss data.

3.4. Electrical Conductivity

The DC conductivity has been found very less in this material and therefore, we examined the variation of AC conductivity w.r.t frequency at different temperatures. **Figure 6** shows the Arrhenius plots of AC conductivity for different frequencies along with the extracted activation energies shown in the figure. It may be noted that the AC conductivity is more at higher frequencies and the corresponding activation energy is reducing when the frequency is increasing.

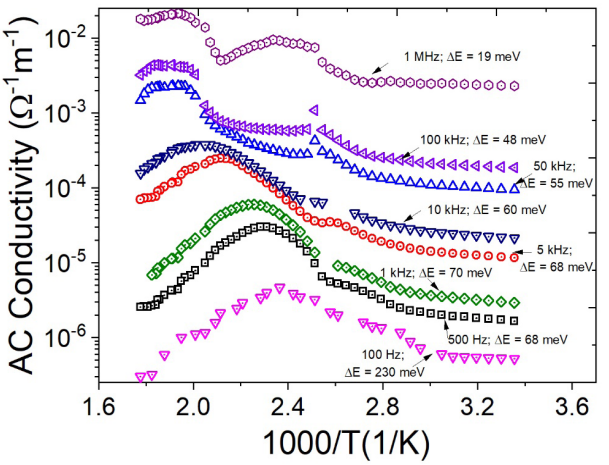

Fig. 6: Electrical conductivity as functions of temperature for different frequency.

The temperature dependence of the AC conductivity curves has been examined separately in **Figures 7(a-h)**. A reasonably good fitting has been obtained with **equation (4)** using the same parameters extracted from the fitting of dielectric constant and dielectric loss data as tabulated in **Table 1**.

The slope changes in the ac conductivity with frequency correspond to the peak in the dielectric loss and are indicative of the changes in the dominant dielectric dispersion mechanisms. The transitions in conductivity from one slope region to another slope region are encircled in **Figures 7(a-h)**. The transition frequencies and the difference in the slopes of the ac conductivity versus frequency curves contain important information about the material [28]. The correlation of these parameters with material characteristics is under investigation at our laboratory.

4. Conclusions

We investigated the dielectric dispersion in a quaternary ceramic material 0.47BNT–0.04BT–0.31PMN–0.18PT having MPB composition,

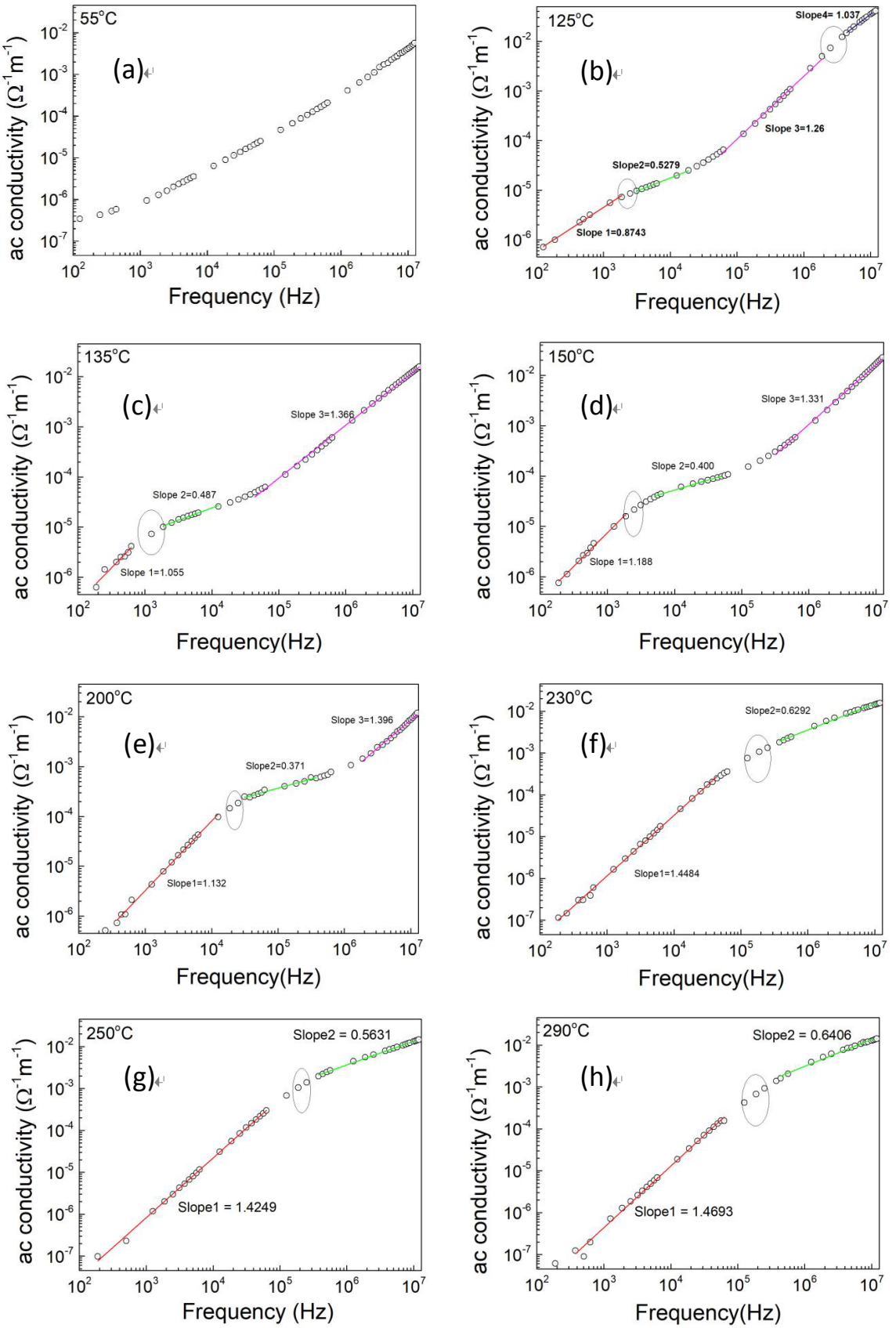

Fig. 7: Electrical conductivity as functions of frequency for different temperatures: (a) 55 °C, (b) 125 °C, (c) 135 °C, (d) 150 °C, (e) 200 °C, (f) 230 °C, (g) 250 °C, (h) 290 °C.

for the first time. The material shows very high dielectric constant of the order of 10^3 to 10^4 along with low dielectric losses over the whole range of frequencies and temperatures used in this study. The material shows two Debye type peaks in dielectric loss versus frequency curves associated with two dielectric dispersions. The first peak occurs at lower frequencies in the range 100 Hz to 10^5 Hz and the second peak occurs at>1 MHz. These peaks shift towards higher frequencies with increasing temperature. An excellent fit of both the peaks has been found with the Debye model. The relaxation times of the two dispersions have about three orders of magnitude difference in their values. The first peak has 2.91 μs characteristic relaxation time with 344 meV activation energy, while second peak has 4.39 ns characteristic relaxation time with 424 meV activation energy. A very high dielectric constant, low dielectric loss, good temperature stability and negligible DC conductivity make this quaternary material a good candidate for fabricating highly efficient devices for a wide variety of applications.

Acknowledgement

Authors are thankful to the principal Hindu College, University of Delhi and Director SSPL, Delhi for their support and encouragement for carrying out this work and publish it.

Declarations

Conflict of Interest

The authors declare that they have no conflict of interest.

Funding

No funding was received for conducting this study.

Data Availability

The data will be made available on reasonable request by the reader.

Author Contributions

All authors have contributed in the interpretation and explanation of the measurement results. Author AJJ did the experimental work of sample preparation and characterization. AS and RSS contributed in the data analysis of reported result and making them in the presentable form. AS prepared the draft manuscript and all authors provided their feedback and suggested appropriate corrections to finalize it.

References

[1] Kazys, R. J., Sliteris, R., Sestoke, J., 2015. Development of air-coupled low frequency ultrasonic transducers and arrays with PMN-32%PT piezoelectric crystals. 2015 IEEE International Ultrasonics Symposium (IUS), 2015, Taipei International Convention Center, Taipai, Taiwan, no. 2, 5–8.

[2] Zhang, Z., Li, F., Chen, R., et al., 2018. High-Performance Ultrasound Needle Transducer Based on Modified PMN-PT Ceramic with Ultrahigh Clamped Dielectric Permittivity. IEEE Transactions on Ultrasonics Ferroelectrics and Frequency Control, 65(2), 223–230. DOI: https://doi.org/10.1109/TUFFC.2017.2778738

[3] Fei, C., Yang, Y., Guo, F., et al., 2018. PMN-PT single crystal ultrasonic transducer with half-concave geometric design for IVUS imaging. IEEE Transactions on Biomedical Engineering, 65(9), 2087–2092. DOI: https://doi.org/10.1109/TBME.2017.2784437

[4] Jiang, Z., Hou, C., Fei, C., et al., 2022. Effects of Composition Segregation in PMN-PT Crystals on Ultrasound Transducer Performance. IEEE Transactions on Ultrasonics Ferroelectrics and Frequency Control, 69(2), 795–802. DOI: https://doi.org/10.1109/TUFFC.2021.3131204

[5] Fang, Z., Tian, X., Zheng, F., et al., 2022. Enhanced piezoelectric properties of Sm3+-modified PMN-PT ceramics and their application in energy harvesting. Ceramics International, 48(6), 7550–7556. DOI: https://doi.org/10.1016/j.ceramint.2021.11.298

[6] Hussain, A., Sinha, N., Bhandari, S., et al., 2016. Synthesis of 0.64Pb(Mg1/3Nb2/3)O3 –0.36PbTiO3 ceramic near morphotropic phase boundary for high performance piezoelectric, ferroelectric and pyroelectric applications. Journal of Asian Ceramic Societies, 4(3), 337–343. DOI: https://doi.org/10.1016/j.jascer.2016.06.004

[7] Roed, E. S., Andersen, K. K., Bring, M., et al., 2019. Acoustic Impedance Matching of PMN-PT/epoxy 1-3 Composites for Underwater Transducers with Usable Bandwidth Restricted by Electrical Power Factor. IEEE International Ultrasonics Symposium (IUS). IUS, 1781–1784. DOI: https://doi.org/10.1109/ULTSYM.2019.8926034

[8] Zhang, Z., 2020. New Sm-PMN-PT Ceramic-Based 2-D Array for Low-Intensity Ultrasound Therapy Application. IEEE Trans. Ultrason. Ferroelectr. Freq. Control, 67(10), 2085–2094, DOI: https://doi.org/10.1109/TUFFC.2020.2979471

[9] Zhang, Q., Su, M., Li, F., Liu, R., Cai, R., Li, G., Jiang, Q., Zhong, H., Shrout, T. R., Zhang, S., Zheng, H., Qiu, W., 2020. A PMN-PT Composite-Based Circular Array for Endoscopic Ultrasonic Imaging. IEEE Transactions on Ultrasonics Ferroelectrics and Frequency Control, 67(11), 2354–2362. DOI: https://doi.org/10.1109/TUFFC.2020.3005029

[10] Ren, M., Xia, W., Xing, J., et al., 2021. The Dielectric and Piezoelectric Properties of the 1-3 Model PMN-PT/PVDF Composite Materials. IEEE International Symposium on Applications of Ferroelectrics (ISAF), 1-3. DOI: https://doi.org/10.1109/ISAF51943.2021.9477353

[11] Chen, H., Mirg, S., Osman, M., et al., 2021. A High Sensitivity Transparent Ultrasound Transducer Based on PMN-PT for Ultrasound and Photoacoustic Imaging. IEEE Sensors Letters, 5(11), 5–8, 2021. DOI: https://doi.org/10.1109/LSENS.2021.3122097

[12] Wang, X., Wang, Y., Zhang, Y., et al., 2021. Enhancement of the piezoelectric property in PMN-PZT/PZT thin films. Ceramics International, 48(9), 3–8. DOI: https://doi.org/10.1016/j.ceramint.2022.01.152

[13] Jia, H., Mi, J., Li, Z., et al., 2022. Improved dielectric and piezoelectric properties of Sm-doped Pb(Mg1/3Nb2/3)O3–Pb(Zn1/3Nb2/3)-PbTiO3 ternary ferroelectric ceramics. Ceramics International, 48(10), 1–6. DOI: https://doi.org/10.1016/j.ceramint.2022.02.013

[14] Castrejón, M. V., Morán, E., Montero, A. R., et al., 2016. Towards Lead-Free Piezoceramics: Facing a Synthesis Challenge. Materials (Basel), 9(21), 1-27. DOI: https://doi.org/10.3390/ma9010021

Yao, K., Chen, S., Guo, K., et al., 2017. Lead-Free Piezoelectric Ceramic Coatings Fabricated by Thermal Spray Process. IEEE Transactions on Ultrasonics, Ferroelectrics, and Frequency Control. 64(11), 1758-1765. DOI: https://doi.org/10.1109/TUFFC.2017.2748154

[16] Gozuacik, N. K., Bayir, M. C., Alkoy, E. M.,et al., 2021. Origin of the Large Field-Induced Strain and Enhanced Energy Storage Response of Rare-Earth-Doped Lead-Free 0.854BNT–0.12BKT–0.026BT Ceramics. IEEE Transactions on Ultrasonics, Ferroelectrics, and Frequency Control, 68(7), 2576-2584. DOI: https://doi.org/10.1109/TUFFC.2021.3063146

[17] Hou, L., Zhou, C., Li, Q., et al., 2022. Giant strain with ultra-low hysteresis by tailoring relaxor temperature and PNRs dynamic in BNT-based lead-free piezoelectric ceramics. Ceramics International, 48(9), 13125-13133. DOI: https://doi.org/10.1016/j.ceramint.2022.01.189

[18] Li, X., Zhang, B., Cao, X., et al., 2022. Large strain response in (Bi0.5Na0.5)TiO3–6BaTiO3-based lead-free ceramics at high temperature. Ceramics International, 48(7), 9051-9058. DOI: https://doi.org/10.1016/j.ceramint.2021.12.088

[19] Shieh, J., Wu, K. C., Chen, C. S., 2007. Switching characteristics of MPB compositions of (Bi0.5Na0.5)TiO3–BaTiO3–(Bi0.5K0.5)TiO3 lead-free ferroelectric ceramics. Acta Materialia, 55(9), 3081-3087.
DOI: https://doi.org/10.1016/j.actamat.2007.01.012

[20] Wongsaenmai, S., Ananta, S., Yimnirun, R., 2009. Effects of addition of BT on structural phase formation and electrical properties of relaxor ferroelectric Pb(In0.5Nb0.5)(1−x)Ti(x)O3 ceramics. Journal of Alloys and Compounds, 474(1–2), 241-245.
DOI: https://doi.org/10.1016/j.jallcom.2008.06.112

[21] Joseph, A. J., Sinha, N., Goel, S., et al, B., 2019. New quaternary BNT–BT–PMN–PT ceramic: ferro/piezo/pyroelectric characterizations. Journal of Materials Science: Materials in Electronics, 30, 2729-12738.
DOI: https://doi.org/10.1007/s10854-019-01637-x

[22] Saxena, A., Hussain, A., Saxena, A., et al., 2022. Dielectric dispersion near the morphotropic phase boundary of 0.64PMN-0.36PT ceramics. Ceramics International, 48(18), 26258-26263.
DOI: https://doi.org/10.1016/j.ceramint.2022.05.307

[23] Wang, D., Bokov, A., Ye, Z. G.,et al., 2016. Subterahertz dielectric relaxation in lead-free Ba(Zr,Ti)O3 relaxor ferroelectrics. Nat. Commun, 7, 11014.
DOI: https://doi.org/10.1038/ncomms11014

[24] Volkov, A. A., Prokhorov, A. S., 2003. Broadband Dielectric Spectroscopy of Solids. Radiophysics and Quantum Electronics 46(8), 657-665.
DOI: https://doi.org/10.1023/B:RAQE.0000024994.15881.c9

[25] Jonscher A. K., Dube, D. C., 1977. Low-Frequency Dielectric Dispersion In Tri-Glycine Sulphate. Ferroelectrics, 17(1), 533–536.
DOI: https://doi.org/10.1080/00150197808236777

[26] Cole, K. S., Cole, R. H., 1941. Dispersion and absorption in dielectrics I. Alternating current characteristics. J. Chem. Phys., 9(4), 341–351.
DOI: https://doi.org/10.1063/1.1750906

[27] Kerstent, O., Schmidt, G., 1986. Dielectric dispersion in pzt ceramics. Ferroelectrics, 67(1), 191–197.
DOI: https://doi.org/10.1080/00150198608245022

[28] Saxena, A., Saxena, A., Saxena, R. S., 2023. Analysing dielectric dispersion of 0.64PMN–0.36PT ceramics using electrical conductivity. Bulletin of Materials Science, 46(124), 1–8.
DOI: https://doi.org/10.1007/s12034-023-02965-9